




An ultrasensitive MnO₂-S,O-doped g-C₃N₄ nanoprobe for “turn-on” detection of glutathione and cell imaging

Chaofan Chai², Xuefang Yang², Xiaohua Yang¹, Chuan Dong³, Wei Bian^{1,4,*} , and Martin M. F. Choi⁵

¹ School of Basic Medical Science, Shanxi Medical University, Taiyuan 030001, China

² College of Pharmacy, Shanxi Medical University, Taiyuan 030001, China

³ Institute of Environmental Science, Shanxi University, Taiyuan 030006, China

⁴ People's Hospital of Lvliang, Lvliang 033099, China

⁵ Bristol Chinese Christian Church, c/o Tyndale Baptist Church, 137-139 Whiteladies Road, Bristol BS8 2QG, UK

Received: 19 November 2021

Accepted: 28 March 2022

Published online:
18 April 2022

© The Author(s), under exclusive licence to Springer Science+Business Media, LLC, part of Springer Nature 2022

ABSTRACT

The utilization of nanomaterial-based probes in detecting glutathione (GSH) and cell imaging has aroused extensive attention owing to the excellent properties of nanoprobos. Herein, we have synthesized manganese dioxide-S, O co-doped graphitic carbon nitride quantum dots (MnO₂-S, O-CNQDs) nanocomposite by in situ synthesis of MnO₂ nanosheets in S,O-CNQDs dispersion solution. It was found that GSH could specifically bind to MnO₂-S, O-CNQDs so that the fluorescence of S, O-CNQDs could be recovered. As such, a “turn-on” MnO₂-S, O-CNQDs nanoprobe can be fabricated and applied to rapidly determine trace amounts of GSH. Under the optimal conditions, MnO₂-S, O-CNQDs shows sensitive response to GSH in the range 10–270 μM with a detection limit of 0.307 μM (*S/N* = 3). The developed MnO₂-S, O-CNQDs probe has demonstrated great potential to detection of GSH in biological samples and glutathione injections. What is more, MTT assay indicates that MnO₂-S, O-CNQDs has low biotoxicity. The non-fluorescence MnO₂-S, O-CNQDs reacts with GSH to recover the fluorescence of S, O-CNQDs in HepG2 cells. Thus, the “turn-on” fluorescence change of MnO₂-S, O-CNQDs offers a potentially useful tool to monitor GSH of cancer cells.

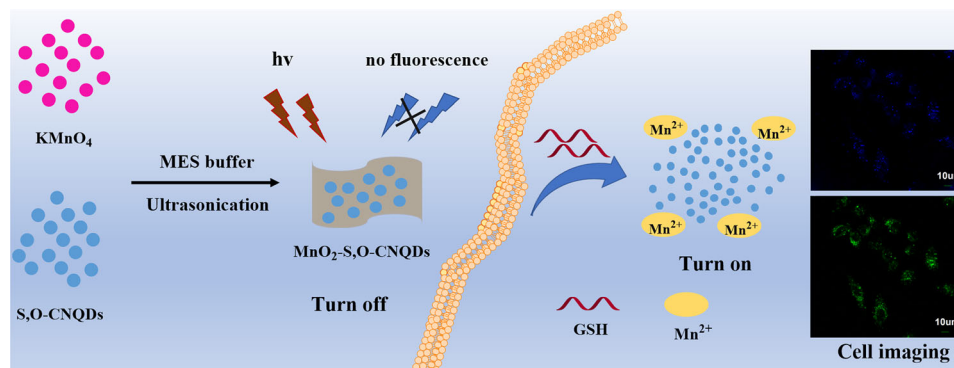
Handling Editor: Andrea de Camargo.

Chaofan Chai and Xuefang Yang have contributed equally to this work.

Address correspondence to E-mail: sxykdx_bianwei@163.com

<https://doi.org/10.1007/s10853-022-07160-5>

GRAPHICAL ABSTRACT

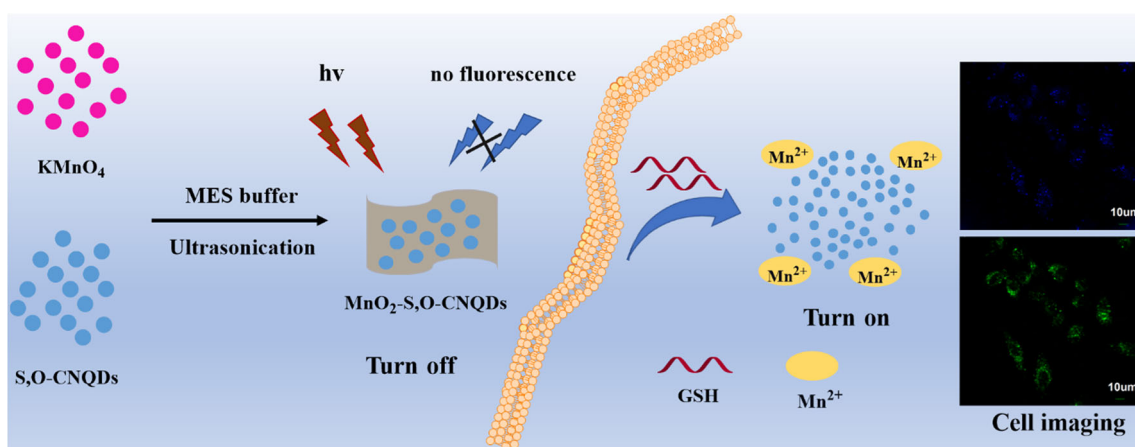


Introduction

Glutathione (GSH) is a tripeptide containing sulfhydryl groups that consists of glutamate, cysteine, and glycine. GSH plays critical roles in physiological functions of human body, which has antioxidant, detoxification, metabolism, and intracellular signal transduction features [1, 2]. However, abnormalities of intracellular GSH levels could cause various diseases such as Parkinson disease [3], liver injury [4], Alzheimer disease [5], and acquired immune deficiency syndrome [6]. Thus, it is essential to detect the level of GSH in human to maintain the quality of life. Up to now, studies indicate that there are several methods for detecting GSH, including high-performance liquid chromatography, mass spectrometry [7], electrochemiluminescence [8], surface enhanced Raman scattering [9], enzyme linked immunosorbent assay [10], and fluorescence spectrometry [11]. Compared with the above-mentioned methods, fluorescence spectrometry has unique advantages of high sensitivity, simplicity, rapidity, and low cost in detection. Among them, nanomaterials are often used as the probes to detect analyte based on spectrofluorometric method. Consequently, the emergence of nanomaterials provides a new opportunity of detecting GSH. So far, nanomaterials such as Au nanocubes, up-conversion luminescent materials, and magnetic metal organic framework have been used to detect GSH, of which, Au nanocubes are limited owing to their higher cost and complex

synthesis procedures [12]. Up-conversion luminescent materials [13] have the disadvantages of the inherently weak photon response and high toxicity, while magnetic metal organic framework has low sensitivity and narrow linear working range to GSH [14]. Over the years, some researchers have dedicated to investigate new advanced nanomaterials or improve those pre-existing nanomaterials for developing simple, rapid, and sensitive GSH nanoprobe [15]. Compared with the above-mentioned nanomaterials, graphitized carbon nitride (g-C₃N₄), as a new type of metal-free semiconductor carbon nanomaterials [16], has attracted extensive attention owing to its obvious advantages of stable, optical, and environment-friendly properties. In addition, g-C₃N₄ has been widely used in the fields of catalysis [17], photoelectrochemistry [18], sensing [19], bioimaging [20], drug delivery [21], and photodynamic therapy [22]. In order to further extend the applications of g-C₃N₄ in these fields, researchers have adopted the surface modification and functionalization to obtain g-C₃N₄ with excellent properties, such as higher quantum yield [23], better photostability [24], better biocompatibility [25], and lower toxicity [26].

MnO₂ nanosheet, as an emerging 2D-layered material, has attracting extensive attention due to its excellent properties including high specific surface area, better light-absorption, fluorescence quenching capability and excellent biocompatibility [27–29]. Yan et al. [27] designed MnO₂ nanosheet-carbon dots sensing platform for sensitive detection of organophosphorus pesticides. Xue et al. [30]



Scheme 1 MnO₂-S, O-CNQDs nanocomposite for GSH assay and reaction mechanism.

synthesized an impedance biosensor based on magnetic nanobead net and MnO₂ nanoflowers for rapid and sensitive detection of foodborne bacteria. Yuan et al. [31] provided MnO₂-nanosheet-modified up-conversion nanosystem to detect H₂O₂ and glucose in blood. Li et al. [32] fabricated morphology-dependent MnO₂/nitrogen-doped graphene nanocomposites for simultaneous detection of trace dopamine and uric acid.

In this work, MnO₂-S, O-CNQDs nanocomposite via in-situ synthesis of MnO₂ nanosheets in S, O-CNQDs dispersion solution has been prepared. Compared with other fluorescent nanomaterials, the combination of doped carbon nitride with higher quantum yield (23.4%) and manganese dioxide can achieve higher detection sensitivity. The nanocomposite does not show fluorescence due to the fluorescence resonance energy transfer (FRET) between MnO₂ nanosheets and S, O-CNQDs. However, when MnO₂-S, O-CNQDs interacts with GSH, the fluorescence of S,O-CNQDs is regenerated, attributed to the specific binding of GSH to MnO₂. Based on this working principle, a rapid, highly selective and low-toxic MnO₂-S, O-CNQDs nanoprobe has been developed to detect intracellular GSH as depicted in Scheme 1.

Our results indicate that MnO₂-S, O-CNQDs is a promising nanoprobe material for quantifying trace amounts of GSH in biological samples as well as monitoring the intracellular level of GSH. It is anticipated that our proposed work could offer a wider application of nanoprobe for multifarious targets via an “off-on” fluorescence detection in biological fields.

Experimental section

Materials and reagents

Thiourea, ethylenediaminetetraacetic acid disodium salt (EDTA-2Na), KMnO₄, and 2-(*N*-morpholino)ethanesulfonic acid (MES) were purchased from Aladdin Co., Ltd. (Shanghai, China). Glutathione, His, Cys, Ala, Thr, Gly, Phe, Trp, Val, glucose, and fructose were bought from Macklin Co., Ltd. (Shanghai, China). Fetal bovine serum (FBS) and 3-(4,5-dimethylthiazol-2-yl)-2,5-diphenyltetrazolium bromide (MTT) were obtained from Sigma Co., Ltd. (St. Louis, MO, USA). Dulbecco’s modified Eagle’s medium (DMEM) was acquired from Gibco Co., Ltd. (St. Louis, MO, USA). Both serum samples and fresh urine samples were obtained from healthy volunteers at The First Hospital of Shanxi Medical University and stored at – 20°C. All reagents were used without further purification. All the solutions were prepared using ultra-pure water.

Measurements

The morphology of the as-synthesized materials was characterized by transmission electron microscopy (TEM) using a JEM 2100-H TEM (Shimadzu, Kyoto, Japan). X-ray diffraction (XRD) was measured on a Bruker D8 Advance powder X-ray diffractometer (Bremen, Germany). X-ray photoelectron spectra (XPS) were performed on a Kratos Axis UltraDL D X-ray photoelectron spectrometer (Hadano, Kanagawa, Japan). The Fourier transform infrared spectra (FT-IR) of S, O-CNQDs, MnO₂, MnO₂-S, O-CNQDs nanocomposite were carried out on a Varian FT-IR-8400 s spectrometer (Agilent Technologies, Santa

Clara, CA, USA). The fluorescence and UV–visible absorption spectra were collected on an FLS920 steady-state transient fluorescence spectrofluorometer (Edinburgh Instruments, Livingston, UK) and Metash 6100 UV/vis spectrophotometer (Meipu Instrument, Shanghai, China), respectively. The samples of solid powder were dried and kept on an FDB-3a vacuum freeze dryer (SIM, Los Angeles, USA). The cellular fluorescence images were obtained from an Olympus FV1000 laser scanning confocal microscope (Leica, Wetzlar, Germany).

Preparation of S,O-CNQDs

S, O-CNQDs were synthesized by a solid-phase reaction method [33]. Firstly, 0.3722 g EDTA-2Na and 0.9134 g thiourea were placed and ground into a mortar to obtain the mixture. The as-obtained powder was then transferred to a crucible and heated at 200 °C for 2 h. After cooling to room temperature, the brown colloidal product was washed three times with ethanol. Then, the brown colloidal product was dissolved in 10 mL ultra-pure water to obtain the brownish-red solution. The solution was centrifuged at 8000 rpm to remove the precipitation, and the supernatant was filtered with a 0.22- μm microporous membrane. Finally, the purified S,O-CNQDs was obtained through dialyzing with a dialysis bag (Solarbio, Beijing, China) of 500 Da molecular weight cutoff for 8 h and followed by freeze-dried in vacuum.

Fabrication of MnO₂-S,O-CNQDs

Five hundred microliters of S, O-CNQDs (3 mg/mL) was pipetted to the centrifuge tube containing 1.5 mL of MES buffer solution (0.10 M, pH 6.0). Then, 1.0 mL of KMnO₄ (15 mM) was dropped into the centrifuge tube and diluted with ultra-pure water to 5.0 mL. Then, the solution was sonicated for 30 min to form a brown colloidal solution. The purified MnO₂-S, O-CNQDs nanocomposite was acquired by centrifugation at 8000 rpm for 10 min and washed several times with ultra-pure water. As a control, bare MnO₂ nanosheets were synthesized using the similar method without S, O-CNQDs. All the experiments were carried out at room temperature.

Fluorescence sensing of GSH

Various concentrations of GSH (0.0–270 μM) were mixed with a known quantity of MnO₂-S, O-CNQDs nanocomposite and ultra-pure water to form 3.0 mL of mixture solution which were kept for 6 min at room temperature. Afterward, the fluorescence emission spectra of the solutions were recorded at an excitation wavelength of 360 nm.

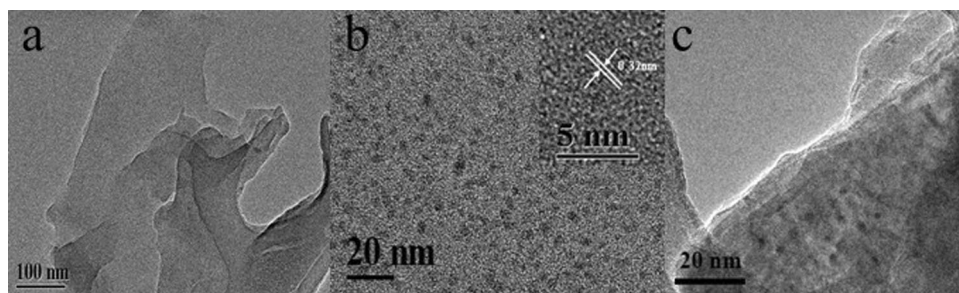
Detection of GSH in human biological samples and glutathione injections

Human serum samples and acetonitrile were mixed with a volume ratio of 1:1. After 3 min, the samples were centrifuged in a 4000 rpm for 30 min to collect the supernatant, which was diluted 100 times with PBS buffer solution (10 mM, pH 6.4) and used for subsequent experiments. The as-prepared samples were mixed with an equal volume of 10 μM , 180 μM , and 250 μM GSH, respectively. Similarly, urine samples were centrifuged to obtain the supernatants which were diluted 1000 times with ultra-water for later use. The rest of the operation was the same as the serum samples. Reduced glutathione injection was a mixture of glutathione and 0.9% sodium chloride injection. Then, the fluorescence spectra of the mixture were measured at an excitation wavelength of 360 nm.

Cytotoxicity assay

The potential cytotoxicity of MnO₂-S, O-CNQDs nanocomposite was evaluated by MTT assay with HepG2 cells. The cell suspensions were seeded onto a 96-well plate (5×10^4 cells per well) with 24-h incubation. After the removal of old medium, each well was washed with PBS for several times. Then, adherent cells of each well were cultivated in 500 μL DMEM containing MnO₂-S, O-CNQDs nanocomposite at various concentrations (0.0–300 $\mu\text{g}/\text{mL}$) for 24 h. The supernatant was removed, and 20 μL MTT solution (5.0 mg/mL) was injected to each well for 4-h incubation. Afterward, the formed formazan crystals were dissolved in 150 μL DMSO by shaking for 10 min. Similarly, a control group was performed without MnO₂-S, O-CNQDs nanocomposite. A blank group was processed in the absence of HepG2 cells and the nanocomposite. The rest operation of the control and blank groups were the same as the

Figure 1 TEM images of **a** MnO₂ nanosheets, **b** S, O-CNQDs, and **c** MnO₂-S, O-CNQDs nanocomposite.



experimental group. Finally, the absorbances were recorded through a microplate reader at 490 nm. The cell viability was calculated according to the equation:

$$\text{Cell viability (\%)} = (\text{OD}_s - \text{OD}_b) / (\text{OD}_c - \text{OD}_b)$$

where OD_s and OD_c represent the absorbances of the experimental and control group cells at 490 nm, respectively. OD_b was recorded in the absence of cells and MnO₂-S, O-CNQDs.

Fluorescence imaging of HepG2 cells

HepG2 cells with a density of 5×10^5 cells in each well were incubated in laser confocal dishes under an atmosphere of 5% CO₂ at 37 °C for 24 h. The cultured cells were divided into the experimental and control groups. In the experimental group, 200 µg/mL of MnO₂-S, O-CNQDs was added into the cells and cultivated for 3 h. Then, the cells were washed with PBS to remove the free MnO₂-S, O-CNQDs, whereas the cells of the control group were preincubated with 500 mM *N*-ethylmaleimide (NEM) for 30 min and washed several times with PBS. The rest of the process was the same as the control group. The fluorescence images of HepG2 cells were performed on a confocal microscope at excitation wavelengths of 405 and 488 nm, respectively.

Results and discussion

Characterization of MnO₂-S, O-CNQDs nanocomposite, S, O-CNQDs and MnO₂ nanosheets

The TEM images of MnO₂, S, O-CNQDs and MnO₂-S, O-CNQDs nanocomposite are displayed in Fig. 1.

Figure 1a shows that MnO₂ forms a lamellar nanosheet structure. The as-prepared S, O-CNQDs having uniform size and good dispersion with

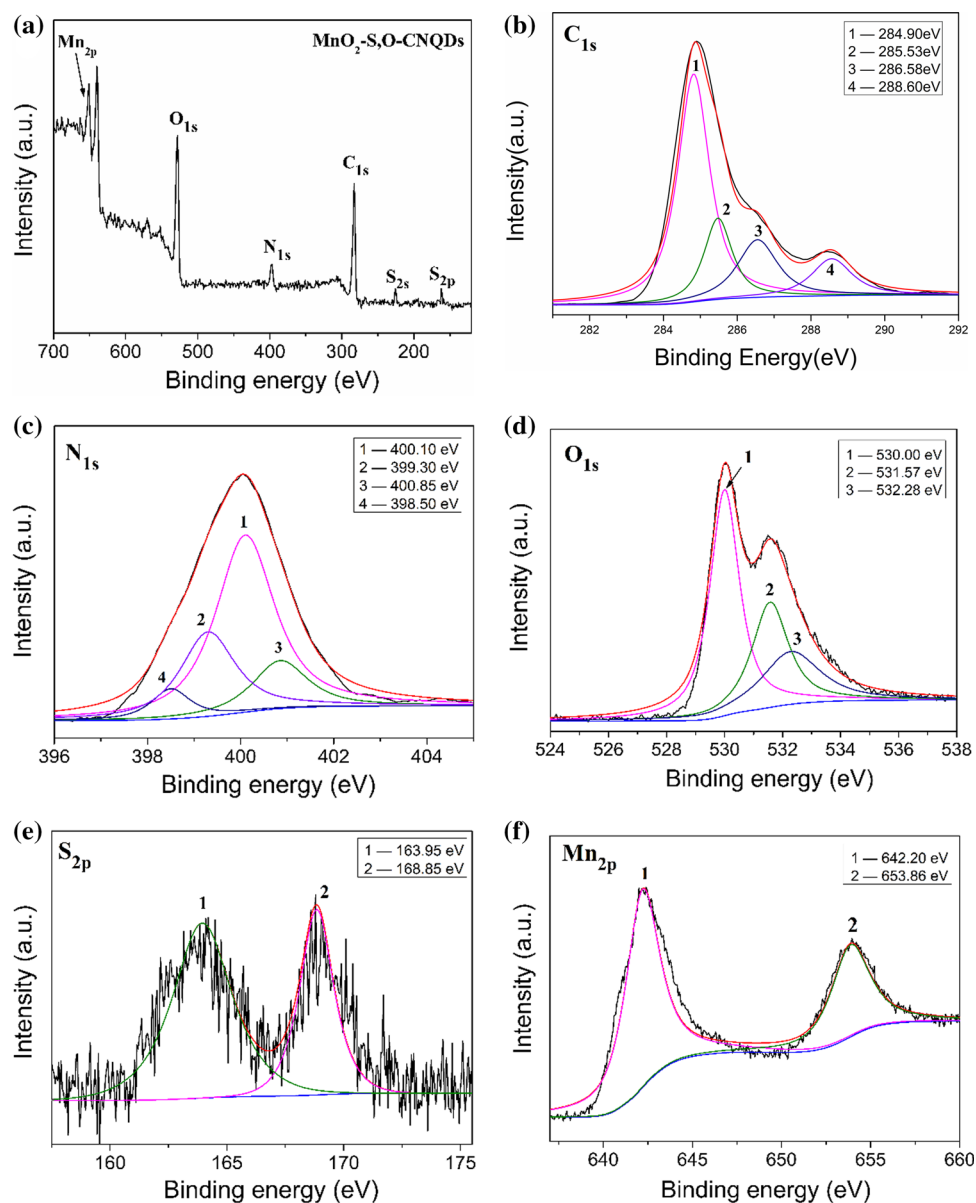
0.32 nm lattice spacing are depicted in Fig. 1b. Furthermore, Fig. 1c shows that the MnO₂-S, O-CNQDs nanocomposite is composed of S, O-CNQDs adhered to the surface of MnO₂ nanosheets. The functional groups of MnO₂-S, O-CNQDs nanocomposite were identified by FT-IR and are shown in Fig. S1. The absorption peak at 3434 cm⁻¹ is attributed to the stretching vibration of O–H [34]. The absorption peak of S–H group is located at 2120 cm⁻¹, while the peaks at 1670 and 1410 cm⁻¹ are originated from the stretching vibration of C=O and the existence of –COOH [35]. Finally, an absorption peak at *ca.* 570 cm⁻¹ of MnO₂-S, O-CNQDs nanocomposite is identified, corresponding to the Mn–O stretching vibration [36].

The chemical compositions of MnO₂-S, O-CNQDs nanocomposite were analyzed by XPS and are depicted in Fig. 2.

Figure 2a shows that MnO₂-S, O-CNQDs contains C, N, O, S, and Mn elements. The C1s fine spectrum of MnO₂-S, O-CNQDs in Fig. 2b exhibits four peaks at 284.90, 285.53, 286.58, and 288.60 eV, attributed to the C=C, C–S, C–O, and C=N bonds, respectively [37]. Figure 2c displays the N 1s spectrum of C₃N₄ XPS which indicates the presence of pyridine-type nitrogen (400.10 eV), C–N (398.50 eV), N–(C)₃ (399.30 eV), and N–H (400.85 eV) in MnO₂-S, O-CNQDs [38]. The fine spectrum of O1s of MnO₂-S, O-CNQDs in Fig. 2d shows three characteristic absorption peaks at 530.00, 531.57, and 532.26 eV, corresponding to the binding energies of O–H, C=O, and C–O bonds [39]. The S2p spectrum of MnO₂-S, O-CNQDs in Fig. 2e has two characteristic absorption peaks, ascribing to the binding energies of C–S bond at the position of 2p_{1/2} (163.95 eV) and 2p_{3/2} (168.85 eV), respectively [34]. Two peaks at 642.27 and 653.86 eV in Fig. 2f belong to the binding energies of Mn2p_{3/2} and Mn2p_{1/2} of MnO₂-S, O-CNQDs nanocomposite, respectively [40].

Figure 3 depicts the XRD patterns of S, O-CNQDs, MnO₂ nanosheets, and MnO₂-S, O-CNQDs

Figure 2 a XPS full spectrum of $\text{MnO}_2\text{-S, O-CNQDs}$ nanocomposite. High-resolution XPS spectra of b C1s , c N1s , d O1s , e S2p , and f Mn2p .



nanocomposite. There are MnO_2 nanosheets with four diffraction peaks at 26.7, 37.2, 45.7, and 56.8° [41]. The diffraction peaks of S, O-CNQDs are centered at 13.4° and 26.8°, corresponding to the in-plane structural packing (100) plane of tri-*s*-triazine units and the typical graphitic interlayer stacking (002) plane, respectively. The diffraction pattern of $\text{MnO}_2\text{-S, O-CNQDs}$ nanocomposite shows that there are no excrement diffraction peaks other than the characteristic peaks of MnO_2 nanosheets and S, O-CNQDs. In essence, the characterization results demonstrate that $\text{MnO}_2\text{-S, O-CNQDs}$ nanocomposite has been successfully prepared.

The stability of $\text{MnO}_2\text{-S, O-CNQDs}$ nanocomposite

The stability of $\text{MnO}_2\text{-S, O-CNQDs}$ nanocomposite was studied under different concentrations of NaCl, UV irradiation, and storage. The experiments were conducted in PBS buffer solution with pH 7.0 at room temperature. Figure S2(a) shows that the fluorescence intensity of $\text{MnO}_2\text{-S, O-CNQDs}$ remains almost unchanged under high concentration of NaCl (1.0 M), indicating that $\text{MnO}_2\text{-S, O-CNQDs}$ have high stability in high-ionic-strength medium. After UV irradiation for 180 min, the fluorescence intensity of $\text{MnO}_2\text{-S, O-CNQDs}$ maintains relatively stable as

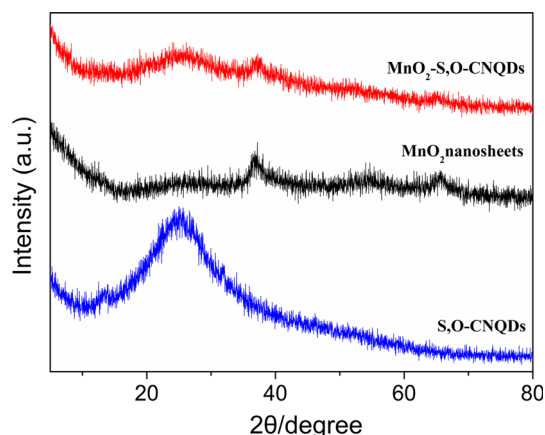


Figure 3 XRD patterns of S, O-CNQDs (blue), MnO₂ nanosheets (black), and MnO₂-S, O-CNQDs nanocomposite (red).

displayed in Fig. S2(b), manifesting that MnO₂-S, O-CNQDs has good photobleaching resistance. The fluorescence intensity of MnO₂-S, O-CNQDs maintains 95% of its initial intensity after 60 d of storage as depicted in Fig. S2(c). These results indicate that MnO₂-S, O-CNQDs nanocomposite possesses good stability which can be a promising fluorescence probe.

The optimization of experimental conditions

In order to obtain a promising fluorescence nanoprobe, the effect of KMnO₄ concentrations for preparing MnO₂-S, O-CNQDs nanocomposite were investigated at room temperature. Figure S3 displays the fluorescence spectra of MnO₂-S, O-CNQDs nanocomposites prepared from various concentrations of KMnO₄ and S, O-CNQDs. It is obvious that the fluorescence of MnO₂-S, O-CNQDs nanocomposite is gradually quenched with the increase in KMnO₄ concentrations. When the concentration of KMnO₄ increases to 15 mM, the fluorescence of S, O-CNQDs drops to the lowest. Further increase in KMnO₄ concentration does not affect the fluorescence of MnO₂-S, O-CNQDs nanocomposite. As such, 15 mM was selected as the optimal concentration of KMnO₄ for preparing MnO₂-S, O-CNQDs nanocomposite.

Detection of GSH

The reaction time of GSH and MnO₂-S, O-CNQDs nanocomposite was optimized. Figure S4 displays the

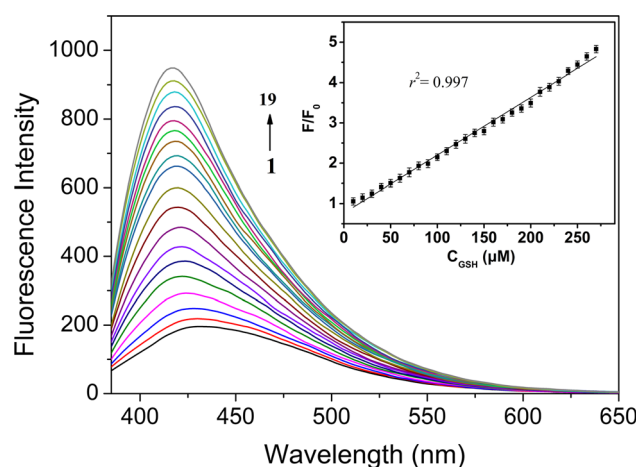


Figure 4 The fluorescence spectra of MnO₂-S, O-CNQDs nanocomposite at various concentrations of GSH. 1–19: 0.0–270 μM. The inset shows the linear relationship between F/F_0 and GSH concentration in the range 10–270 μM.

plot of F_0/F against t (reaction time) of GSH (50 μM) and MnO₂-S, O-CNQDs nanocomposite (5.0 mg/mL), where F_0 and F are the initial fluorescence intensity and intensity of MnO₂-S, O-CNQDs nanocomposite at t , respectively. It can be observed that F_0/F increases rapidly after the addition of GSH and then reaches the highest at 6.0 min. Further increase in reaction time does not increase the F_0/F . As a result, 6.0 min was chosen as the optimal reaction time in the subsequent work.

To verify the applicability of our proposed “turn-on” nanoprobe for detection of GSH, the fluorescence of MnO₂-S, O-CNQDs at various GSH concentrations was investigated and is shown in Fig. 4. The fluorescence of MnO₂-S, O-CNQDs gradually increases with the increase in concentration of GSH. The inset of Fig. 4 shows the linear relationship ($r^2 = 0.997$) between F/F_0 and GSH concentration (10–270 μM), where F_0 and F are the fluorescence intensities of MnO₂-S, O-CNQDs in the absence and presence of GSH. The detection limit is determined to be 0.307 μM ($S/N = 3$).

In order to compare with MnO₂-S, O-CNQDs, a solution containing MnO₂ and S, O-CNQDs was also used for GSH detection. The corresponding results are presented in Fig. S5. When different concentrations of GSH are added to the solutions, the fluorescence of the solutions is restored gradually. The linear relationship ($r^2 = 0.998$) is obtained between F/F_0 and the concentration of GSH in the range 20–80 μM with a detection limit of 7.14 μM. Compared to the solution containing MnO₂ and S,

Table 1 Different fluorescence nanoprobes for detecting GSH

Nanoprobe	Linear range (μM)	Detection limit (nM)	References
Carbon dots-MnO ₂	1.0–10.0	300	[42]
Two-photon multi-emissive fluorescent probe	10.0–50.0	540	[43]
Conjugated microporous polymer	0.2–20.0	60	[44]
Carbon dots	1.0–10.0 and 25.0–150.0	260	[45]
CoOOH nanosheets	33.0–1300.0	1370	[46]
MnO ₂ -S, O-CNQDs	10.0–270.0	307	This work

O-CNQDs, MnO₂-S, O-CNQDs shows a wider linear range and lower detection limit. In order to determine repeatability of measurement, 50, 100, and 150 μM GSH are used to determine their F_0/F at 10 repeat measurements. The relative standard deviation of the fluorescence intensity of MnO₂-S, O-CNQDs is 4.20%, indicating that the nanoprobe possesses good repeatability of fluorescence intensity. Table 1 compares the analytical performance of our proposed nanoprobe with other reported fluorescence nanoprobes for GSH detection. The analytical performance of our nanoprobe is comparable with other fluorescence nanoprobes for GSH detection. In addition, our nanoprobe displays a wide linear range and reasonable detection limit.

Selectivity and interference assays of MnO₂-S, O-CNQDs nanocomposite for GSH

In order to evaluate the selectivity and interference of MnO₂-S, O-CNQDs nanocomposite toward GSH, the reaction of nanocomposite with the interfering substances including common metal ions, anions, amino acids, and sugars at concentrations of 200 μM under the optimal experimental conditions was investigated and is shown in Fig. 5. Figure 5a shows that MnO₂-S, O-CNQDs nanocomposite responds to GSH only, whereas the interferents do not give any significant effect. When GSH is co-excited with 30-fold concentrations of various interferents, the F/F_0 shows almost no significant change as depicted in Fig. 5b. Compared to other published nanoprobes for GSH detection, our proposed MnO₂-S, O-CNQDs have better selectivity and anti-interference ability. These results indicate that MnO₂-S, O-CNQDs nanocomposite could be an ideal “turn-on” probe for selective detection of GSH in the presence of interferents.

Study on the interaction mechanism between MnO₂-S, O-CNQDs nanocomposite and GSH

Fluorescence resonance energy transfer is a phenomenon of non-radiative energy transfer between two fluorescence chromophores, which are energy donor and energy acceptor through the dipole–dipole interaction. The process of FRET manifests that the fluorescence lifetime of the donor is shortened and the fluorescence intensity of the acceptor is increased [47]. In general, the following conditions are satisfied

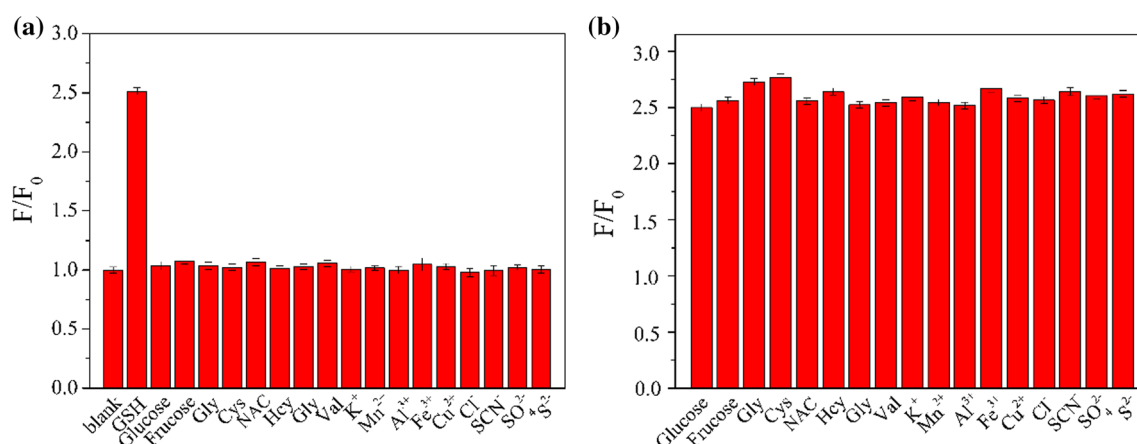


Figure 5 The selectivity **a** and interference **b** of MnO₂-S, O-CNQDs nanocomposite for GSH and non-target substances. NAC: N-acetyl-L-cysteine ($n = 3$).

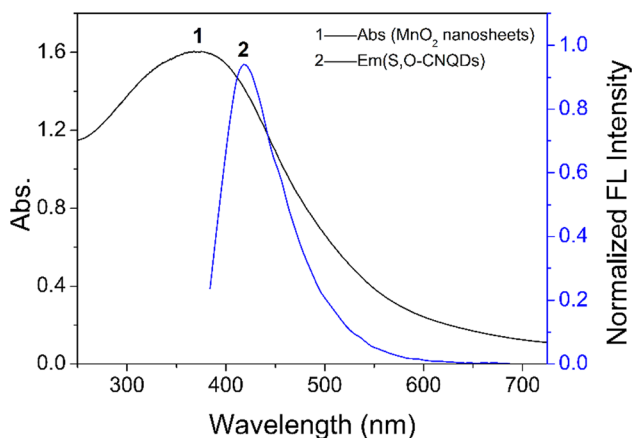


Figure 6 UV–visible absorption spectrum of MnO₂ nanosheets (black) and the fluorescence emission spectrum of S, O-CNQDs (blue).

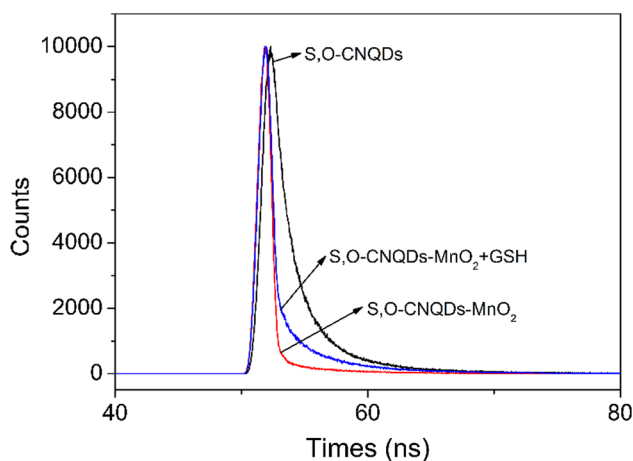


Figure 7 The time-resolved fluorescence spectra of S, O-CNQDs (3.0 mg/mL), MnO₂-S,O-CNQDs (3.0 mg/mL) and MnO₂-S,O-CNQDs (3.0 mg/mL) with GSH (180 μM).

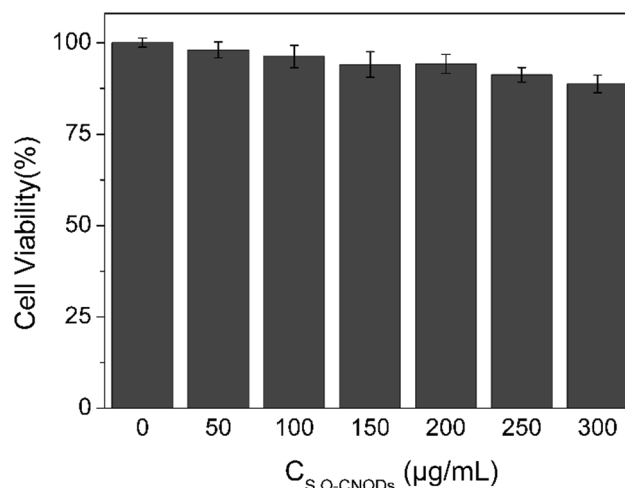


Figure 8 Cell viability of HepG2 cells incubated with MnO₂-S, O-CNQDs nanocomposite (0.0–300 μg/mL) for 12 h (*n* = 3).

in order to have FRET to take place. First, the emission spectrum of donor overlaps with the absorption spectrum of acceptor. Secondly, the distance of the donor and acceptor is in the range 1–10 nm. FRET efficiency (*E*) can be calculated between S, O-CNQDs and MnO₂ using Eq. (1):

$$E = 1 - \frac{\tau_{D-A}}{\tau_A} = \frac{R_0^6}{R^4 R_0^6} \tag{1}$$

τ_{D-A} and τ_A are before and after the fluorescence lifetimes on the combination of energy donor and receptor, respectively. *R* represents the distance between energy donor and receptor. *R*₀ means the critical distance of Förster, which can be calculated by Eq. (2):

Table 2 Determination of GSH in human serum, urine samples and reduced glutathione injection

Sample	Measured (μM)	Spiked (μM)	Found (μM)	Recovery (%)	RSD (<i>n</i> = 3)
Serum	13.16	10.00	23.01	98.5	1.95
		180.00	192.99	99.9	2.62
		250.00	264.32	100.5	3.15
Urine	12.74	10.00	22.44	97.0	2.73
		180.00	195.81	101.7	1.26
		250.00	269.53	102.7	2.97
Reduced glutathione injection	15.63	10.00	25.52	98.9	2.74
		180.00	198.01	101.3	2.83
		250.00	262.64	98.8	3.21

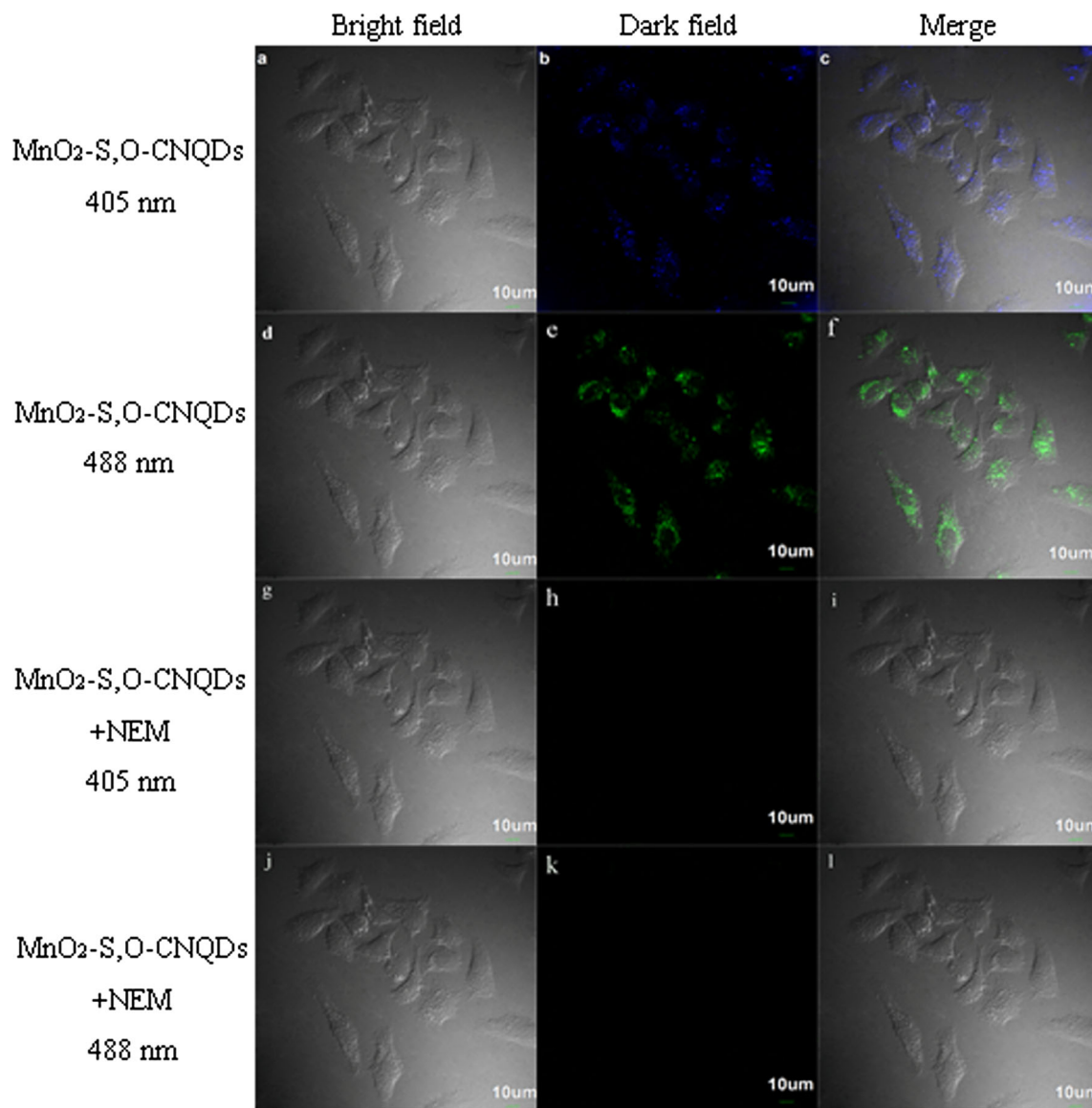


Figure 9 Laser scanning confocal fluorescence images of HepG2 cells of the experimental group which were incubated with 200 $\mu\text{g/mL}$ $\text{MnO}_2\text{-S, O-CNQDs}$ in bright field (**a** and **d**), bright field (**b**: 405 nm and **e**: 488 nm) and merge (**c** and **f**). Laser scanning confocal fluorescence images of HepG2 cells of the control group which were incubated with 500 mM NEM and 200 $\mu\text{g/mL}$ $\text{MnO}_2\text{-S, O-CNQDs}$ in bright field (**g** and **j**), bright field (**h**: 405 nm and **k**: 488 nm) and merge (**i** and **l**).

$$R_0^6 = 8.97 \times 10^{23} \cdot \kappa^2 \cdot n^{-4} \cdot QY_D \cdot J(\lambda) \quad (2)$$

κ^2 represents the dipole orientation factor in the range of 0–4 ($\kappa^2 = 2/3$). n indicates the refractive index of the solvent, QY_D shows the fluorescence quantum yield of donor in the absence of receptor.

In order to clarify the fluorescence quenching mechanism of S, O-CNQDs induced by MnO_2 , the UV–visible absorption spectrum of MnO_2 nanosheets

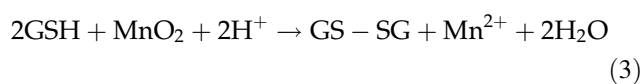
as the acceptor and the fluorescence emission spectrum of S, O-CNQDs as the donor were investigated. Figure 6 shows the UV–visible absorption spectrum of MnO_2 nanosheets which largely overlaps with the fluorescence emission spectrum of S, O-CNQDs, indicating that FRET may take place between MnO_2 nanosheets and S,O-CNQDs.

The time-resolved fluorescence spectra of S, O-CNQDs (3.0 mg/mL), $\text{MnO}_2\text{-S, O-CNQDs}$

(3.0 mg/mL) and MnO₂-S, O-CNQDs (3.0 mg/mL) with GSH (180 μM) were determined and are shown in Fig. 7.

The fluorescence lifetimes of S, O-CNQDs and MnO₂-S, O-CNQDs nanocomposite are determined to be 2.5 and 1.6 ns, respectively. The distance (*R*) between the MnO₂ nanosheets and S, O-CNQDs is 3.83 nm, and transfer efficiency (*E*) of FRET is 0.36 which were calculated according to Eqs. (1) and (2). These results indicate that S, O-CNQDs is the donor, while MnO₂ is the receptor. Thus, the fluorescence quenching mechanism of MnO₂-induced S, O-CNQDs is mainly governed by FRET.

In this work, S, O-CNQDs were deposited on the surface of MnO₂ nanosheets to form the non-fluorescence MnO₂-S, O-CNQDs nanocomposite owing to FRET. However, in the presence of GSH, MnO₂ nanosheets are reduced into Mn²⁺ and GSH is rapidly oxidized into its oxidized form (GSSG) according to Eq. (3) [48]. Meanwhile, S, O-CNQDs are released and its fluorescence is restored.



Determination of GSH in real samples

In order to evaluate the practicability of the fabricated MnO₂-S, O-CNQDs nanocomposite, it was applied to detect GSH in real samples. First, different concentrations of GSH were spiked into the diluted biological samples and the GSH injections, respectively. Table 2 summarizes the determination and recovery of GSH in human serum, urine and reduced glutathione injection samples. The recoveries are in the range 97.0–102.7% for biological samples. The results indicate that MnO₂-S, O-CNQDs nanocomposite could be a promise fluorescence probe to detect GSH in real samples.

Cytotoxicity assay and fluorescence imaging in living cells

Cytotoxicity assay should be taken into consideration before applying the nanoprobe for imaging of living cells. The cytotoxicity of MnO₂-S, O-CNQDs nanocomposite was tested through a standard MTT method. When the concentration of nanocomposite reaches 300 μg/mL, HepG2 cells still keep over 88% viability as depicted in Fig. 8. The results reveal that

our nanocomposite has low cytotoxicity and good biocompatibility. Owing to the excellent properties of the nanocomposite, it was applied to monitor the intracellular GSH level in conjunction with a laser scanning confocal microscope.

Figure 9 displays the blue fluorescence ($\lambda_{\text{ex}} = 405 \text{ nm}$) and green fluorescence ($\lambda_{\text{ex}} = 488 \text{ nm}$) of the HepG2 cells which have been incubated with 200 μg/mL MnO₂-S, O-CNQDs nanocomposite.

When HepG2 cells are treated with 500 mM NEM as the control group, almost no fluorescence is observed under the laser scanning confocal microscope. These results demonstrate that the nanocomposite with good fluorescence properties can be applied as a “turn-on” probe for bioimaging of GSH in living cells.

Conclusion

In the work, the fluorescence of S, O-CNQDs (an energy donor) was efficiently quenched by MnO₂ (an energy acceptor) based on the FRET effect. The interaction between GSH and MnO₂ has a restoring effect on the fluorescence intensity of S, O-CNQDs. As such, a new fluorescence “turn-on” probe for detecting GSH using MnO₂-S, O-CNQDs nanocomposite has been developed. The probe displays a good detection capability for GSH in aqueous solution with a wide working range 10–270 μM and a detection limit of 0.307 μM. Our proposed nanoprobe can be applied to real samples (serum, urine and GSH injection solution) for GSH detection with satisfactory results. In addition, the MnO₂-S, O-CNQDs nanocomposite can be used for intracellular imaging of GSH. All these results suggest that MnO₂-S, O-CNQDs nanocomposite is a promising material which can be utilized for determining GSH in biological, injection samples and human cells. It is anticipated that researchers will continue to explore more novel nanomaterials as the fluorescence probes for effective, low-cost and high-sensitive determination of different analytes.

Acknowledgements

Financial support from the Natural Science Foundation of Shanxi Province of China (201901D111210), Key Research Project of Science and Technology in

JinZhong-Social Development Projects (Y213003), Special Project of Lvliang for Introduced High-level Science and Technology Talents (2021RC-2-33), National Natural Science Foundation of China (21874087), and Transverse Scientific Research Project of Shanxi University (2F022019056) is gratefully acknowledged.

Author contributions

CC and XY were involved in the conceptualization, methodology, investigation, formal analysis, data curation, and writing—original draft preparation. XY contributed to the resources, visualization, and investigation. CD contributed to the resources, and visualization. WB was involved in the conceptualization, supervision, funding acquisition, validation, and writing—original draft preparation. MMFC contributed to the writing—review and editing.

Declarations

Conflict of interest The authors declare that they have no known competing financial interests or personal relationships that could have appeared to influence the work reported in this paper.

Supplementary Information: The online version contains supplementary material available at <https://doi.org/10.1007/s10853-022-07160-5>.

References

- [1] Kong RM, Ma L, Han X, Ma C, Qu F, Xia L (2020) Hg²⁺-mediated stabilization of G-triplex based molecular beacon for label-free fluorescence detection of Hg²⁺, reduced glutathione, and glutathione reductase activity. *Spectrochim Acta A Mol Biomol Spectrosc* 228:117855. <https://doi.org/10.1016/j.saa.2019.117855>
- [2] Lv H, Zhen C, Liu J, Yang P, Hu L, Shang P (2019) Unraveling the potential role of glutathione in multiple forms of cell death in cancer therapy. *Oxid Med Cell Longev* 2019:3150145. <https://doi.org/10.1155/2019/3150145>
- [3] Smeyne M, Smeyne RJ (2013) Glutathione metabolism and Parkinson's disease. *Free Radic Biol Med* 62:13–25. <https://doi.org/10.1016/j.freeradbiomed.2013.05.001>
- [4] Lu SC, Mato JM, Espinosa-Diez C, Lamas S (2016) MicroRNA-mediated regulation of glutathione and methionine metabolism and its relevance for liver disease. *Free Radic Biol Med* 100:66–72. <https://doi.org/10.1016/j.freeradbiomed.2016.03.021>
- [5] Pocernich CB, Butterfield DA (2012) Elevation of glutathione as a therapeutic strategy in Alzheimer disease. *Biochim Biophys Acta* 5:625–630. <https://doi.org/10.1016/j.bbadis.2011.10.003>
- [6] Perricone C, De Carolis C, Perricone R (2009) Glutathione: a key player in autoimmunity. *Autoimmun Rev* 8(8):697–701. <https://doi.org/10.1016/j.autrev.2009.02.020>
- [7] Iwasaki Y, Saito Y, Nakano Y, Mochizuki K, Sakata O, Ito R, Saito K, Nakazawa H (2009) Chromatographic and mass spectrometric analysis of glutathione in biological samples. *J Chromatogr B Analyt Technol Biomed Life Sci* 877(28):309–317. <https://doi.org/10.1016/j.jchromb.2009.07.001>
- [8] Hanko M, Svorc L, Plankova A, Mikus P (2019) Overview and recent advances in electrochemical sensing of glutathione: a review. *Anal Chim Acta* 1062:1–27. <https://doi.org/10.1016/j.aca.2019.02.052>
- [9] Saha A, Jana NR (2013) Detection of cellular glutathione and oxidized glutathione using magnetic-plasmonic nanocomposite-based “turn-off” surface enhanced Raman scattering. *Anal Chem* 85(19):9221–9228. <https://doi.org/10.1021/ac4019457>
- [10] Wawegama NK, Browning GF, Kanci A, Marenda MS, Markham PF (2014) Development of a recombinant protein-based enzyme-linked immunosorbent assay for diagnosis of *Mycoplasma bovis* infection in cattle. *Clin Vaccine Immunol* 21(2):196–202. <https://doi.org/10.1128/cvi.00670-13>
- [11] Chen JA, Zhang ZY, Gao J, Tan JH, Gu XF (2019) Design of fluorescent probes with optimized responsiveness and selectivity to GSH. *Tetrahedron Lett* 60(18):1226–1230. <https://doi.org/10.1016/j.tetlet.2019.03.051>
- [12] Li Y, Jiang L, Zou Y, Song Z, Jin S (2021) Highly reproducible SERS sensor based on self-assembled Au nanocubic monolayer film for sensitive and quantitative detection of glutathione. *Appl Surf Sci* 540:148381. <https://doi.org/10.1016/j.apsusc.2020.148381>
- [13] Zhang L, Ling B, Wang L, Chen H (2017) A near-infrared luminescent Mn²⁺-doped NaYF₄:Yb, Tm/Fe³⁺ upconversion nanoparticles redox reaction system for the detection of GSH/Cys/AA. *Talanta* 172:95–101. <https://doi.org/10.1016/j.talanta.2017.05.031>
- [14] Zhang Y, Zhang W, Chen K, Yang Q, Hu N, Suo Y, Wang J (2018) Highly sensitive and selective colorimetric detection of glutathione via enhanced Fenton-like reaction of magnetic metal organic framework. *Sens Actuators B Chem* 262:95–101. <https://doi.org/10.1016/j.snb.2018.01.221>
- [15] Chu S, Wang H, Du Y, Yang F, Yang L, Jiang C (2020) Portable smartphone platform integrated with a nanoprobe-

- based fluorescent paper strip: visual monitoring of glutathione in human serum for health prognosis. *ACS Sustain Chem Eng* 8(22):8175–8183. <https://doi.org/10.1021/acssuschemeng.0c00690>
- [16] Pan J, Zheng Z, Yang J, Wu Y, Lu F, Chen Y, Gao W (2017) A novel and sensitive fluorescence sensor for glutathione detection by controlling the surface passivation degree of carbon quantum dots. *Talanta* 166:1–7. <https://doi.org/10.1016/j.talanta.2017.01.033>
- [17] He F, Wang Z, Li Y, Peng S, Liu B (2020) The nonmetal modulation of composition and morphology of g-C₃N₄-based photocatalysts. *Appl Catal B* 269:118828. <https://doi.org/10.1016/j.apcatb.2020.118828>
- [18] Wang L, Tong Y, Feng J, Hou J, Li J, Hou X, Liang J (2019) g-C₃N₄-based films: a rising star for photoelectrochemical water splitting. *Sustain Mater Technol* 19:e00089. <https://doi.org/10.1016/j.susmat.2018.e00089>
- [19] Bansod B, Kumar T, Thakur R, Rana S, Singh I (2017) A review on various electrochemical techniques for heavy metal ions detection with different sensing platforms. *Biosens Bioelectron* 94:443–455. <https://doi.org/10.1016/j.bios.2017.03.031>
- [20] Zhang X, Xie X, Wang H, Zhang J, Pan B, Xie Y (2012) Enhanced photoresponsive ultrathin graphitic-phase C₃N₄ nanosheets for bioimaging. *J Am Chem Soc* 135(1):18–21. <https://doi.org/10.1021/ja308249k>
- [21] Habibi Jouybari M, Hosseini S, Mahboobnia K, Boloursaz LA, Moradi M, Irani M (2019) Simultaneous controlled release of 5-FU, DOX and PTX from chitosan/PLA/5-FU/g-C₃N₄-DOX/g-C₃N₄-PTX triaxial nanofibers for breast cancer treatment in vitro. *Colloids Surf B Biointerfaces* 179:495–504. <https://doi.org/10.1016/j.colsurfb.2019.04.026>
- [22] Taheri H, Unal MA, Sevim M, Gurcan C, Ekim O, Ceylan A, Syrgiannis Z, Christoforidis KC et al (2020) Photocatalytically active graphitic carbon nitride as an effective and safe 2D material for in vitro and in vivo photodynamic therapy. *Small* 16(10):e1904619. <https://doi.org/10.1002/smll.201904619>
- [23] Zhao Z, Zheng H, Wang Y, Cai X, Mao L, Zhang J (2019) Hydrogen atom etching induced large-size ultrathin g-C₃N₄ nanosheets for enhanced photoluminescence. *J Lumin* 206:660–665. <https://doi.org/10.1016/j.jlumin.2018.10.080>
- [24] Naidu PP, Raghavendra G, Ojha S, Paplal B (2019) Effect of g-C₃N₄ nanofiller as filler on mechanical properties of multidirectional glass fiber epoxy hybrid composites. *J Appl Polym Sci* 137(9):48413. <https://doi.org/10.1002/app.48413>
- [25] Yang J, Liang Y, Li K, Yang G, Wang K, Xu R, Xie X (2019) Cyano and potassium-rich g-C₃N₄ hollow tubes for efficient visible-light-driven hydrogen evolution. *Catal Sci Technol* 9(13):3342–3346. <https://doi.org/10.1039/c9cy00925f>
- [26] Rong M, Cai Z, Xie L, Lin C, Song X, Luo F, Wang Y, Chen X (2016) Study on the ultrahigh quantum yield of fluorescent P, O-g-C₃N₄ nanodots and its application in cell imaging. *Chemistry* 22(27):9387–9395. <https://doi.org/10.1002/chem.201601065>
- [27] Yan X, Song Y, Zhu C, Li H, Du D, Su X, Lin Y (2018) MnO₂ nanosheet-carbon dots sensing platform for sensitive detection of organophosphorus pesticides. *Anal Chem* 90(4):2618–2624. <https://doi.org/10.1021/acs.analchem.7b04193>
- [28] Garg D, Mehta A, Mishra A, Basu S (2018) A sensitive turn on fluorescent probe for detection of biothiols using MnO₂@carbon dots nanocomposites. *Spectrochim Acta A Mol Biomol Spectrosc* 192:411–419. <https://doi.org/10.1016/j.saa.2017.11.041>
- [29] Yang J, Huang Z, Hu Y, Ge J, Li J, Li Z (2018) A facile fluorescence assay for rapid and sensitive detection of uric acid based on carbon dots and MnO₂ nanosheets. *New J Chem* 42(18):15121–15126. <https://doi.org/10.1039/c8nj02607f>
- [30] Xue L, Guo R, Huang F, Qi W, Liu Y, Cai G, Lin J (2020) An impedance biosensor based on magnetic nanobead net and MnO₂ nanoflowers for rapid and sensitive detection of foodborne bacteria. *Biosens Bioelectron* 173:112800. <https://doi.org/10.1016/j.bios.2020.112800>
- [31] Yuan J, Cen Y, Kong XJ, Wu S, Liu CL, Yu RQ, Chu X (2015) MnO₂-nanosheet-modified upconversion nanosystem for sensitive turn-on fluorescence detection of H₂O₂ and glucose in blood. *ACS Appl Mater Interfaces* 7(19):10548–10555. <https://doi.org/10.1021/acsami.5b02188>
- [32] Li Q, Xia Y, Wan X, Yang S, Cai Z, Ye Y, Li G (2020) Morphology-dependent MnO₂/nitrogen-doped graphene nanocomposites for simultaneous detection of trace dopamine and uric acid. *Mater Sci Eng C Mater Biol Appl* 109:110615. <https://doi.org/10.1016/j.msec.2019.110615>
- [33] Zhou J, Yang Y, Zhang CY (2013) A low-temperature solid-phase method to synthesize highly fluorescent carbon nitride dots with tunable emission. *Chem Commun* 49(77):8605–8607. <https://doi.org/10.1039/c3cc42266f>
- [34] Wang H, Lu Q, Li M, Li H, Liu Y, Li H, Zhang Y, Yao S (2018) Electrochemically prepared oxygen and sulfur co-doped graphitic carbon nitride quantum dots for fluorescence determination of copper and silver ions and biothiols. *Anal Chim Acta* 1027:121–129. <https://doi.org/10.1016/j.aca.2018.03.063>
- [35] Lu YC, Chen J, Wang AJ, Bao N, Feng JJ, Wang W, Shao L (2015) Facile synthesis of oxygen and sulfur co-doped graphitic carbon nitride fluorescent quantum dots and their application for mercury(II) detection and bioimaging.

- J Mater Chem C 3(1):73–78. <https://doi.org/10.1039/c4tc02111h>
- [36] Wu M, Hou P, Dong L, Cai L, Chen Z, Zhao M, Li J (2019) Manganese dioxide nanosheets: from preparation to biomedical applications. *Int J Nanomed* 14:4781–4800. <https://doi.org/10.2147/ijn.s207666>
- [37] Sundari R, Alva S, Sebayang D, Wahyudi H, Jonit S, Kamaruddin A (2018) Characterization of fabricated MnO₂-amberlite photocatalyst by FTIR, XRD and SEM for alizarin removal. *IOP Conf Ser Mater Science Eng* 343:012003. <https://doi.org/10.1088/1757-899X/343/1/012003>
- [38] Zhou X, Shao C, Li X, Wang X, Guo X, Liu Y (2018) Three dimensional hierarchical heterostructures of g-C₃N₄ nanosheets/TiO₂ nanofibers: controllable growth via gas-solid reaction and enhanced photocatalytic activity under visible light. *J Hazard Mater* 344:113–122. <https://doi.org/10.1016/j.jhazmat.2017.10.006>
- [39] Li Y, Li P, Wang J, Yang Y, Yao W, Wei Z, Wu J, Yan X et al (2018) Water soluble graphitic carbon nitride with tunable fluorescence for boosting broad-response photocatalysis. *Appl Catal B* 225:519–529. <https://doi.org/10.1016/j.apcatb.2017.12.017>
- [40] Feng X, Cox DF (2018) Oxidation of MnO(100) and NaMnO₂ formation: Characterization of Mn²⁺ and Mn³⁺ surfaces via XPS and water TPD. *Surf Sci* 675:47–53. <https://doi.org/10.1016/j.susc.2018.04.022>
- [41] Wang Y, Zhu M, Jiang E, Hua R, Na R, Li QX (2017) A simple and rapid turn on ESIPT fluorescent probe for colorimetric and ratiometric detection of biothiols in living cells. *Sci Rep* 7(1):4377. <https://doi.org/10.1038/s41598-017-03901-8>
- [42] Cai QY, Li J, Ge J, Zhang L, Hu YL, Li ZH, Qu LB (2015) A rapid fluorescence “switch-on” assay for glutathione detection by using carbon dots-MnO₂ nanocomposites. *Biosens Bioelectron* 72:31–36. <https://doi.org/10.1016/j.bios.2015.04.077>
- [43] Luo W, Zhang S, Meng Q, Zhou J, Jin R, Long X, Tang YP, Guo H (2021) A two-photon multi-emissive fluorescent probe for discrimination of Cys and Hcy/GSH via an aromatic substitution-rearrangement. *Talanta* 224:121833. <https://doi.org/10.1016/j.talanta.2020.121833>
- [44] Wang S, Wang M, Liu Y, Meng X, Ye Y, Song X, Liang Z (2021) Novel D-π-A conjugated microporous polymer as visible light-driven oxidase mimic for efficient colorimetric detection of glutathione. *Sens Actuators B Chem* 326:128808. <https://doi.org/10.1016/j.snb.2020.128808>
- [45] Li L, Shi L, Jia J, Eltayeb O, Lu W, Tang Y, Dong C, Shuang S (2020) Dual photoluminescence emission carbon dots for ratiometric fluorescent GSH sensing and cancer cell recognition. *ACS Appl Mater Interfaces* 12(16):18250–18257. <https://doi.org/10.1021/acsami.0c00283>
- [46] Li J, Jiao L, Xu W, Yan H, Chen G, Wu Y, Hu L, Gu W (2021) Cobalt oxyhydroxide nanosheets integrating with metal indicator enable sensitive detection of glutathione. *Sens Actuators B Chem* 329:129247. <https://doi.org/10.1016/j.snb.2020.129247>
- [47] Yan X, Song Y, Zhu C, Song J, Du D, Su X, Lin Y (2016) Graphene quantum dot-MnO₂ nanosheet based optical sensing platform: a sensitive fluorescence “Turn Off-On” nanosensor for glutathione detection and intracellular imaging. *ACS Appl Mater Interfaces* 8(34):21990–21996. <https://doi.org/10.1021/acsami.6b05465>
- [48] Chen Y, Cong H, Shen Y, Yu B (2020) Biomedical application of manganese dioxide nanomaterials. *Nanotechnology* 31(20):202001. <https://doi.org/10.1088/1361-6528/ab6fe1>

Publisher's Note Springer Nature remains neutral with regard to jurisdictional claims in published maps and institutional affiliations.